KAERI/TR-1652/2000

Non-Linear Triangle-based Polynomial Expansion Nodal Method for Hexagonal Core Analysis

(육방형 노심 해석을 위한 비선형 삼각형 기반 다항식 전개법)

Korea Atomic Energy Research Institute

PLEASE BE AWARE THAT
ALL OF THE MISSING PAGES IN THIS DOCUMENT
WERE ORIGINALLY BLANK

제 출 문

한국원자력연구소장 귀하

본 보고서를 " Non-Linear Triangle-based Polynomial Expansion Nodal Method for Hexagonal Core Analysis" 에 관한 기술보고서로 제출합니다.

2000 년 10 월

연구기관명 : 한국원자력연구소

참여연구원

주 저 자: 조 진 영 (일체형원자로노심설계기술개발)

공 동 저 자: 조 병 오 (일체형원자로노심설계기술개발)

주 한 규 (일체형원자로노심설계기술개발)

지 성 균 (일체형원자로노심설계기술개발)

박 상 윤 (일체형원자로노심설계기술개발)

요 약

이 연구에서는 육방형 노심 설계/해석을 위한 비선형 다항식전개법을 MASTER코드에 적용하여 그 성능을 평가하였다. 삼각형노드에 대한 다항식전개 노달법은 3차원 프리즘 노드에 대한 고차다항식전개법과 유사한 방법으로 축방향으로의 중성자누설항을 중성자 확산방정식에서 중성자원으로 두어 고차다항식전개법에서의 축방향 노드간의 연계를 차단한 방법이다. 축방향으로의 중성자원은 노달전개법(NEM)을 도입하여 구하였다. 그리고 MASTER 코드의 노드구조와 일치시키기 위해 6개의 삼각형으로 구성된 하나의 육각형 노드에 대한 다항식 전개법의 해를 가우스소거법에 의해 직접 푸는 방식을 채택하였다.

거시격자 유한차분법의 해를 효율적으로 구하기 위한 방법으로는 Stabilized Bi-Conjugate Gradient(BiCG) 알고리듬과 Wielandt eigenvalue shift 방법이 채택되었다. 그리고 BiCG 알고리듬의 선행자(preconditioner)를 구하기 위해서 불완전 LU인자법(incomplete LU factorization)이 사용되었으며 이를 3차원 공간에 적용하기 위해 symmetric Gauss-Seidel Factorization 방법이 사용되었다.

비선형 다항식 전개법의 정확도 및 계산속도 검증은 다양한 고유치 계산문제와 2개의 과도해석문제를 통해 수행되었다. 고유치문제에 대한 적용결과 비선형 다항식전개법은 모든 문제에서 15pcm 이내의 고유치 오차를 그리고 최대 1% 이내의 집합체 출력오차를 보여 매우 정확한 방법임을 보였으며, VVER-440 3차원 문제를 5초이내에 계산하여 매우 빠른 방법임을 보였다. 과도해석문제에 대해서는 다른 코드 결과와 매우 유사한 결과를 보였으며 수분이내에 계산을 완료하여 매우 빠름을 확인하였다.

Abstract

This report is for the implementation of triangle-based polynomial expansion nodal (TPEN) method to MASTER code in conjunction with the coarse mesh finite difference(CMFD) framework for hexagonal core design and analysis. The TPEN method is a variation of the higher order polynomial expansion nodal (HOPEN) method that solves the multi-group neutron diffusion equation in the hexagonal-z geometry. In contrast with the HOPEN method that represents the intranodal solution in a three-dimensional domain with a truncated polynomial expansion, only two-dimensional intranodal expansion is considered in the TPEN method for a triangular domain. The axial dependence of the intranodal flux is incorporated separately here and it is determined by the nodal expansion method (NEM) for a hexagonal node. For the consistency of node geometry of the MASTER code which is based on hexagon, TPEN solver is coded to solve one hexagonal node which is composed of 6 triangular nodes directly with Gauss elimination scheme.

To solve the CMFD linear system efficiently, stabilized bi-conjugate gradient(BiCG) algorithm and Wielandt eigenvalue shift method are adopted. And for the construction of the efficient preconditioner of BiCG algorithm, the incomplete LU(ILU) factorization scheme which has been widely used in two-dimensional problems is used. To apply the ILU factorization scheme to three-dimensional problem, a symmetric Gauss-Seidel Factorization scheme is used.

In order to examine the accuracy of the TPEN solution, several eigenvalue benchmark problems and two transient problems, i.e., a realistic VVER1000 and VVER440 rod ejection benchmark problems, were solved and compared with respective references. The results of eigenvalue benchmark problems indicate that non-linear TPEN method is very accurate showing less than 15 pcm of eigenvalue errors and 1% of maximum power errors, and fast enough to solve the three-dimensional VVER-440 problem within 5 seconds on 733MHz PENTIUM-III. In the case of the transient problems, the non-linear TPEN method also shows good results within a few minute of computing time on the same platform machine.

Table of Contents

List of Tables

List of Figures

1. Introduction

The triangle-based polynomial expansion nodal (TPEN) method is a variation of the higher order polynomial expansion nodal (HOPEN) method [1] that solves the multi-group neutron diffusion equation in the hexagonal-z geometry. In contrast with the HOPEN method that represents the intranodal solution in a three-dimensional domain with a truncated polynomial expansion, only two-dimensional intranodal expansion is considered in the TPEN method for a triangular domain. The axial dependence of the intranodal flux is incorporated separately here and it is determined by the nodal expansion method (NEM). For the consistency of node geometry of the MASTER code which is based on hexagon, TPEN solver is coded to solve one hexagonal node which is composed of 6 triangular node directly by Gauss elimination scheme.

To solve the coarse-mesh finite difference(CMFD) linear system efficiently, stabilized bi-Conjugate gradient(BiCG) algorithm is adopted, and for the construction of the efficient preconditioner, the incomplete LU(ILU) factorization scheme which has been widely used in two-dimensional problems is used. To apply the ILU factorization scheme to three-dimensional problem, a symmetric Gauss-Seidel Factorization scheme is used.

The TPEN method is implemented to the MASTER code in conjunction with the CMFD framework for hexagonal core design and analysis. This work is completed by introducing data transfer module between the MASTER code and non-linear TPEN module.

In chapter 2, the CMFD linear system solver is presented with the ILU factorization scheme.

In chapter 3, the TPEN method is presented first assuming that the axial leakage information is available. And then, from the TPEN solution for the triangular geometry, a response matrix type formulation of TPEN is derived for a hexagon. In the next section, the method of representing the radial dependence of the axial leakage term and the method for the corner point flux calculation is described. The way of CMFD adjoint flux calculation and core reactivity are also described in chapter 3. In chapter 4, the implementation of the non-linear TPEN method to the MASTER code and control logics for the CMFD linear system are descrbed. In chapter 5, the benchmark results are described for the various eigenvalue and two transient problems.

2. CMFD Linear System Solver

2.1 CMFD linear system

In the CMFD formulation the surface-average current at the interface of any two nodes is represented by the following relation in terms of the two node-average fluxes:

$$J = -\tilde{D}(\phi_R - \phi_L) - \hat{D}(\phi_R + \phi_L) \qquad (2.1\text{-}1)$$

where D-tilde is the base nodal coupling coefficient that is determined by the ordinary finite difference approximation (namely first order accurate) and D-hat is the corrective nodal coupling coefficient that is iteratively determined by a higher order nodal solver. The CMFD linear system is a set of nodal balance equation involving the above relation.

In order to solve the CMFD linear system efficiently, the preconditioned Bi-Conjugate Gradient Stabilized (BiCG-STAB) algorithm[2] is adopted because of it's well known performance for the nonlinear and transient problems. For the construction of efficient preconditioner, the incomplete LU(ILU) factorization scheme[3] which has been widely used in two-dimensional problems is used. To apply the ILU factorization scheme to three-dimensional problem, symmetric Gauss-Seidel factorization scheme[4] is used. In the following section ILU factorization scheme is described.

2.2 Incomplete LU Factorization

Fig.2-1 shows the incomplete LU factorization scheme. In this scheme, the generated LU matrixes have the same fill-in structure with the original matrix. To make the fill-in structure of LU be the same with the original matrix, the gauss elimination is applied to non-zero elements of original matrix.

```
function [L,U]=ilu(A_org);
% ILU Factorization
A=A_org;
[n,nn]=size(A);
for i=2:n
    for k=1:i-1
        if(A(i,k)~=0)
            m=A(i,k)/A(k,k);
            A(i,k)=m;
            for j=k+1:n
                if(A(i,j)~=0)
                    A(i,j)=A(i,j)-m*A(k,j);
                end
            end
        end
    end
end

U=triu(A);
L=A-U+sparse(eye(n));
```

Figure 2-1 Incomplete LU factorization Algorithm

3. The Triangle-based Polynomial Expansion Nodal Kernel

3.1 The Triangle-based Polynomial Expansion Nodal Method

The derivation of the TPEN method starts with defining various types of unknowns in a triangular computational node. Fig. 3-1 displays a triangular node and the unknowns defined in it. The x, u, and p symbols in this figure denote the local planar coordinate axes with the origin placed at the center of the node. The y, v, q are the perpendicular coordinates to these axes, respectively. The nine unknowns defined are the volume average flux, first-order x- and y-moments, three surface average fluxes and three corner fluxes, respectively. The followings specify the nine unknowns in detail:

Volume average flux: $\bar{\phi}_g^m = \frac{1}{V^m}\int\int \phi_g^m(x,y)\,dx\,dy$,

First order x-moment: $\tilde{\phi}_{gx}^m = \frac{2\sqrt{3}}{3h}\frac{1}{V^m}\int\int x\phi_g^m(x,y)\,dx\,dy$, (3.1-1)

First order y-moment: $\tilde{\phi}_{gy}^m = \frac{2}{h}\frac{1}{V^m}\int\int y\phi_g^m(x,y)\,dx\,dy$,

Surface average flux: $\bar{\phi}_{gx}^m = \frac{1}{h}\int \phi_g^m(x,y)\Big|_{x=\frac{\sqrt{3}}{6}h} dy$ (same definition for the surfaces perpendicular to the p and u directions), and

Corner flux: $\phi_x^m = \phi_x^m(x,y)\Big|_{\left(\frac{\sqrt{3}}{3}h,0\right)}$ (same definition for the corner points located on the p and u axes).

A truncated polynomial expansion of the intranodal flux in the two-dimensional domain that is consistent with the nine unknowns can be set as:

$$\phi_g^m(x,y) = c_{g0}^m + a_{gx}^m x + a_{gy}^m y + b_{gx}^m x^2 + b_{gu}^m u^2 + b_{gp}^m p^2 + c_{gx}^m x^3 + c_{gu}^m u^3 + c_{gp}^m p^3, \qquad (3.1\text{-}2)$$

with nine expansion coefficients.

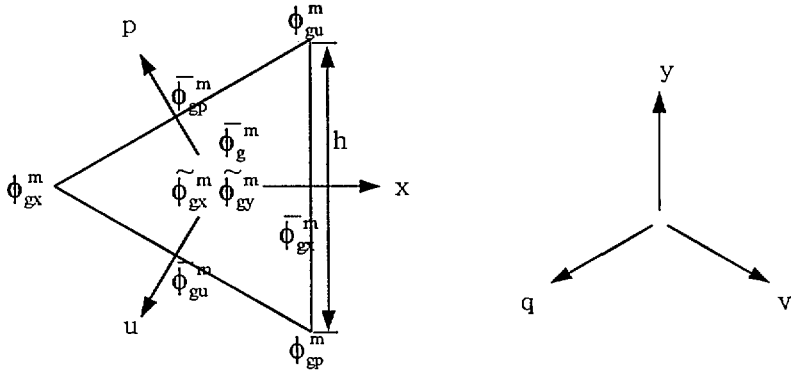

$$V^m = \text{node volume} = \frac{\sqrt{3}}{4}h^2$$

Figure 3-1. Unknowns and Coordinates for the TPEN method

Using the definitions of the unknowns specified in Eq. (3.1-1), one can show that the expansion coefficients in Eq. (3.1-2) are related to the unknowns in a unique way. Namely, the expansion coefficients can be expressed in terms of the unknowns as:

$$c_{g0}^m = \frac{1}{27}\left\{\phi_{gx}^m + \phi_{gu}^m + \phi_{gp}^m - 12\left(\bar{\phi}_{gx}^m + \bar{\phi}_{gu}^m + \bar{\phi}_{gp}^m\right) + 60\bar{\phi}_g^m\right\},$$

$$a_{gx}^m = \frac{2\sqrt{3}}{9h}\left\{\left(2\phi_{gx}^m - \phi_{gu}^m - \phi_{gp}^m\right) + 90\tilde{\phi}_{gx}^m\right\},$$

$$a_{gy}^m = \frac{2}{3h}\left\{-\left(\phi_{gu}^m - \phi_{gp}^m\right) + 30\tilde{\phi}_{gy}^m\right\},$$

$$b_{gx}^m = -\frac{4}{3h^2}\left\{\left(\phi_{gu}^m + \phi_{gp}^m\right) - 12\bar{\phi}_{gx}^m + 10\bar{\phi}_g^m + 60\tilde{\phi}_{gx}^m\right\},$$

$$b_{gu}^{m} = -\frac{4}{3h^2}\left\{\left(\phi_{gp}^{m} + \phi_{gx}^{m}\right) - 12\bar{\phi}_{gu}^{m} + 10\bar{\phi}_{g}^{m} - 30\left(\tilde{\phi}_{gx}^{m} + \tilde{\phi}_{gy}^{m}\right)\right\}, \tag{3.1-3}$$

$$b_{gp}^{m} = -\frac{4}{3h^2}\left\{\left(\phi_{gx}^{m} + \phi_{gu}^{m}\right) - 12\bar{\phi}_{gp}^{m} + 10\bar{\phi}_{g}^{m} - 30\left(\tilde{\phi}_{gx}^{m} - \tilde{\phi}_{gy}^{m}\right)\right\},$$

$$c_{gx}^{m} = -\frac{16\sqrt{3}}{9h^3}\left\{-3\phi_{gx}^{m} - \left(\phi_{gu}^{m} + \phi_{gp}^{m}\right) + 9\bar{\phi}_{gx}^{m} + 3\left(\bar{\phi}_{gu}^{m} + \bar{\phi}_{gp}^{m}\right) - 10\bar{\phi}_{g}^{m} - 60\tilde{\phi}_{gx}^{m}\right\},$$

$$c_{gu}^{m} = -\frac{16\sqrt{3}}{9h^3}\left\{-3\phi_{gu}^{m} - \left(\phi_{gp}^{m} + \phi_{gx}^{m}\right) + 9\bar{\phi}_{gu}^{m} + 3\left(\bar{\phi}_{gp}^{m} + \bar{\phi}_{gx}^{m}\right) - 10\bar{\phi}_{g}^{m} + 30\left(\tilde{\phi}_{gx}^{m} + \tilde{\phi}_{gy}^{m}\right)\right\},$$

$$c_{gp}^{m} = -\frac{16\sqrt{3}}{9h^3}\left\{-3\phi_{gp}^{m} - \left(\phi_{gx}^{m} + \phi_{gu}^{m}\right) + 9\bar{\phi}_{gp}^{m} + 3\left(\bar{\phi}_{gx}^{m} + \bar{\phi}_{gu}^{m}\right) - 10\bar{\phi}_{g}^{m} + 30\left(\tilde{\phi}_{gx}^{m} - \tilde{\phi}_{gy}^{m}\right)\right\}.$$

Once the polynomial approximation of the intranodal flux distribution is made, the nine unknowns are uniquely determined. For this, there should be a sufficient number of constraints that the unknowns must satisfy. The constraints are constructed by using the following two-dimensional neutron diffusion equation that reads:

$$\begin{aligned} -D_{g}^{m}\left(\frac{\partial^2}{\partial x^2} + \frac{\partial^2}{\partial y^2}\right)\phi_{g}^{m}(x,y) + \Sigma_{rg}^{m}\phi_{g}^{m}(x,y) \\ = \frac{\chi_g}{k_{eff}}\sum_{g'}\nu\Sigma_{fg'}^{m}\phi_{g'}^{m}(x,y) + \sum_{g'}\Sigma_{sgg'}^{m}\phi_{g'}^{m}(x,y) + S_{gz}^{m}(x,y), \end{aligned} \tag{3.1-4}$$

where $S_{gz}^{m}(x,y)$ is axial source distribution which comes from axial leakage and described in Section 3.4.

The first constraint is the nodal balance equation that reads:

$$\frac{1}{V^m}\iint\langle \text{Eq.}(3.1-4)\rangle\, dx\, dy. \tag{3.1-5}$$

By inserting Eq.(3.1-2) into (3.1-4) and using Eq.(3.1-3), the nodal neutron balance equation is

obtained as the following in terms of node average and surface fluxes: :

$$\left(80\frac{D_g^m}{h^2}+\Sigma_{rg}^m\right)\bar{\phi}_g^m=\frac{\chi_g}{k_{eff}}\sum_{g'}\nu\Sigma_{fg'}^m\bar{\phi}_{g'}^m+\sum_{g'}\Sigma_{sgg'}^m\bar{\phi}_{g'}^m+\bar{S}_{gz}^m$$
$$+32\frac{D_g^m}{h^2}\left(\bar{\phi}_{gx}^m+\bar{\phi}_{gu}^m+\bar{\phi}_{gp}^m\right)-\frac{16}{3}\frac{D_g^m}{h^2}\left(\phi_{gx}^m+\phi_{gu}^m+\phi_{gp}^m\right) \tag{3.1-6}$$

where $\bar{S}_{gz}^m$ is averaged axial source and described in Section 3.4.

The second constraint is constructed using the weighted residual method with x as a weighting function, namely:

$$\frac{2\sqrt{3}}{3h}\frac{1}{V^m}\iint x\langle \text{Eq.}(3.1-4)\rangle\,dx\,dy. \tag{3.1-7}$$

This yields the x-weighted residual equation as:

$$\left(80\frac{D_g^m}{h^2}+\Sigma_{rg}^m\right)\tilde{\phi}_{gx}^m=\frac{\chi_g}{k_{eff}}\sum_{g'}\nu\Sigma_{fg'}^m\tilde{\phi}_{g'x}^m+\sum_{g'}\Sigma_{sgg'}^m\tilde{\phi}_{g'x}^m+\tilde{S}_{gzx}^m$$
$$+\frac{8}{3}\frac{D_g^m}{h^2}\left(2\bar{\phi}_{gx}^m-\bar{\phi}_{gu}^m-\bar{\phi}_{gp}^m\right)-\frac{8}{9}\frac{D_g^m}{h^2}\left(2\phi_{gx}^m-\phi_{gu}^m-\phi_{gp}^m\right) \tag{3.1-8}$$

where $\tilde{S}_{gzx}^m$ is the x-moment of the source as described in Section 3.4.

The y-moment of flux can be obtained similarly with y as a weighting function:

$$\left(80\frac{D_g^m}{h^2}+\Sigma_{rg}^m\right)\tilde{\phi}_{gy}^m=\frac{\chi_g}{k_{eff}}\sum_{g'}\nu\Sigma_{fg'}^m\tilde{\phi}_{g'y}^m+\sum_{g'}\Sigma_{sgg'}^m\tilde{\phi}_{g'y}^m+\tilde{S}_{gzy}^m$$
$$-8\frac{D_g^m}{h^2}\left(\bar{\phi}_{gu}^m-\bar{\phi}_{gp}^m\right)+\frac{8}{3}\frac{D_g^m}{h^2}\left(\phi_{gu}^m-\phi_{gp}^m\right) \tag{3.1-9}$$

where $\tilde{S}_{gzy}^m$ is the y-moment of the source.

The fourth constraint comes from the continuity condition of the surface average net current at the interface of the two adjacent nodes, namely (refer to Fig. 3-2 for the definition of the symbols):

$$\bar{J}_{gx}^m=\bar{J}_{gx}^{m+1}. \tag{3.1-10}$$

The net current from node m at the interface between the node m and $m+1$ is defined as:

$$\bar{J}_{gx}^m=\frac{1}{h}\int -D_g^m\frac{\partial}{\partial x}\phi_g^m(x,y)\Big|_{x=\frac{\sqrt{3}}{6}h}dy. \tag{3.1-11}$$

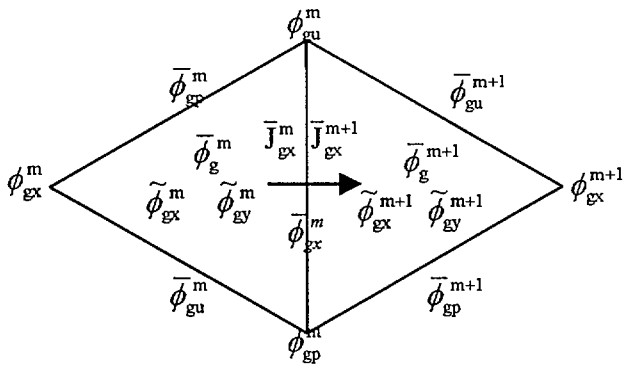

Figure 3-2. Two adjacent nodes and nodal unknowns

By inserting Eq.(3.1-2) to Eq.(3.1-11) and using Eq.(3.1-3), the net current can be expressed as a function of nodal unknowns of node m as:

$$\bar{J}_{gx}^{m} = \frac{\sqrt{3}}{3}\frac{D_g^m}{h}\left\{2\phi_{gx}^{m} + \phi_{gu}^{m} + \phi_{gp}^{m} - 24\bar{\phi}_{gx}^{m} + 20\bar{\phi}_{g}^{m} + 120\tilde{\phi}_{gx}^{m}\right. . \tag{3.1-12}$$

The net current from the node m+1 is obtained similarly. The net current continuity condition for the surface flux can be obtained by inserting these relations into Eq. (3.1-10) as:

$$\begin{aligned} 24\left(D_g^m + D_g^{m+1}\right)\bar{\phi}_{gx}^{m} = {} & 2\left(D_g^m\phi_{gx}^{m} + D_g^{m+1}\phi_{gx}^{m+1}\right) + \left(D_g^m + D_g^{m+1}\right)\left(\phi_{gu}^{m} + \phi_{gp}^{m}\right) \\ & + 20\left(D_g^m\bar{\phi}_{g}^{m} + D_g^{m+1}\bar{\phi}_{g}^{m+1}\right) + 120\left(D_g^m\tilde{\phi}_{gx}^{m} + D_g^{m+1}\tilde{\phi}_{gx}^{m+1}\right). \end{aligned} \tag{3.1-13}$$

The current continuity condition is applied to the three surfaces of the triangle, and thus it provides three constraints.

The last constraints come from a condition imposed at each corner point of the triangle. It is the net leakage balance condition as illustrated in Fig. 3-3. At a corner point, there are six nodes surrounding the corner point (c). For the simplicity of expression, the x-y coordinates are defined at each local triangle and x-direction is defined as the direction from the center point to the outer surface. By referring to Fig. 2-3, the net leakage balance condition is expressed as:

$$\sum_{m=1}^{6} L_{gx}^{m} = 0. \tag{3.1-14}$$

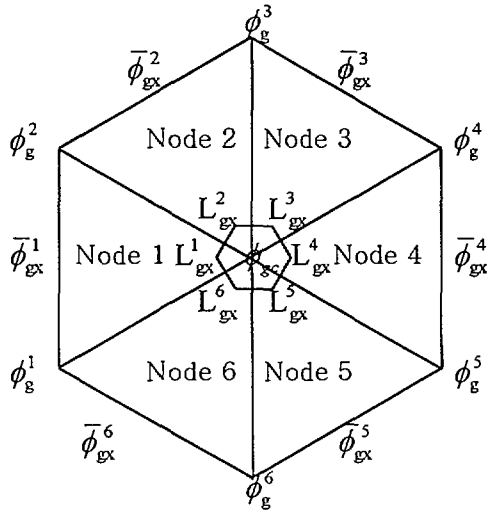

Figure 3-3. Six surrounding nodes of point c and unknowns

The net leakage from node 1 at the center point of Fig.3-3 is defined as:

$$L^1_{gx} = -D^1_g\left(\frac{d}{du}+\frac{d}{dp}\right)\phi^1_g(x,y)\Big|_{\left(-\frac{\sqrt{3}}{3}h,0\right)}. \tag{3.1-15}$$

By inserting Eq.(3.1-2) into Eq.(3.1-15) and using Eq.(3.1-3), the net leakage can be expressed as a function of nodal unknowns of node 1 as:

$$L^1_{gx} = 4\sqrt{3}\frac{D^1_g}{h}\left\{-\phi_{gc}+\bar{\phi}^1_{gx}-15\tilde{\phi}^1_{gx}\right\}. \tag{3.1-16}$$

The final expression of the net leakage balance condition is obtained by inserting Eq.(3.1-16) to Eq.(3.1-14) as:

$$\left(D_g^1+D_g^2+D_g^3+D_g^4+D_g^5+D_g^6\right)\phi_{gc}=D_g^1\bar{\phi}_{gx}^1+D_g^2\bar{\phi}_{gx}^2+D_g^3\bar{\phi}_{gx}^3+D_g^4\bar{\phi}_{gx}^4 +D_g^5\bar{\phi}_{gx}^5+D_g^6\bar{\phi}_{gx}^6-15\left(D_g^1\tilde{\phi}_{gx}^1+D_g^2\tilde{\phi}_{gx}^2+D_g^3\tilde{\phi}_{gx}^3+D_g^4\tilde{\phi}_{gx}^4+D_g^5\tilde{\phi}_{gx}^5+D_g^6\tilde{\phi}_{gx}^6\right). \quad (3.1\text{-}17)$$

3.2 Response Matrix Formulation on a Hexagonal Node

In this section, the TPEN method is applied to a hexagonal node to derive a response matrix that relates the outgoing partial currents to the incoming partial currents specified at the six surfaces of the hexagon. Fig. 3-4 shows 6 triangular nodes consisting a hexagonal node. For this hexagonal node, 6 incoming partial currents and 6 corner point fluxes are specified as the boundary conditions. Applying the TPEN to the six triangles yields 31 unknowns consisting of 6 average fluxes, 6 x-moments, 6 y-moments, 6 inner surface fluxes, 6 outgoing partial currents and 1 center point flux.

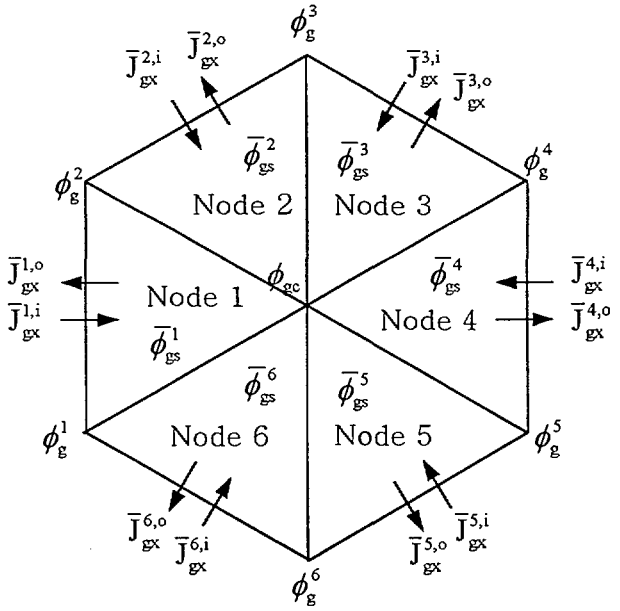

Figure 3-4. Boundary Conditions and Nodal Unknowns on a Hexagonal Node for TPEN

To determine 6 node average fluxes, 6 x-moments, 6 y-moments, 6 inner surface fluxes and one center point flux, Eq.(3.1-6), Eq.(3.1-8), Eq.(3.1-9), Eq.(3.1-13) and Eq.(3.1-17) are used. Eq.(3.1-13) is also used to determine 6 outgoing partial currents. The resulting linear system to determine these unknowns is derived as:

$$
\begin{bmatrix}
\begin{bmatrix} a_1 & 0 & 0 & 0 & 0 & 0 \\ 0 & a_1 & 0 & 0 & 0 & 0 \\ 0 & 0 & a_1 & 0 & 0 & 0 \\ 0 & 0 & 0 & a_1 & 0 & 0 \\ 0 & 0 & 0 & 0 & a_1 & 0 \\ 0 & 0 & 0 & 0 & 0 & a_1 \end{bmatrix} & \begin{bmatrix} 0 & 0 & 0 & 0 & 0 & 0 \\ 0 & 0 & 0 & 0 & 0 & 0 \\ 0 & 0 & 0 & 0 & 0 & 0 \\ 0 & 0 & 0 & 0 & 0 & 0 \\ 0 & 0 & 0 & 0 & 0 & 0 \\ 0 & 0 & 0 & 0 & 0 & 0 \end{bmatrix} & \begin{bmatrix} 0 & 0 & 0 & 0 & 0 & 0 \\ 0 & 0 & 0 & 0 & 0 & 0 \\ 0 & 0 & 0 & 0 & 0 & 0 \\ 0 & 0 & 0 & 0 & 0 & 0 \\ 0 & 0 & 0 & 0 & 0 & 0 \\ 0 & 0 & 0 & 0 & 0 & 0 \end{bmatrix} & \begin{bmatrix} a_2 & a_3 & 0 & 0 & 0 & 0 \\ 0 & a_2 & a_3 & 0 & 0 & 0 \\ 0 & 0 & a_2 & a_3 & 0 & 0 \\ 0 & 0 & 0 & a_2 & a_3 & 0 \\ 0 & 0 & 0 & 0 & a_2 & a_3 \\ a_3 & 0 & 0 & 0 & 0 & a_2 \end{bmatrix} & \begin{bmatrix} a_4 & 0 & 0 & 0 & 0 & 0 \\ 0 & a_4 & 0 & 0 & 0 & 0 \\ 0 & 0 & a_4 & 0 & 0 & 0 \\ 0 & 0 & 0 & a_4 & 0 & 0 \\ 0 & 0 & 0 & 0 & a_4 & 0 \\ 0 & 0 & 0 & 0 & 0 & a_4 \end{bmatrix} & \begin{bmatrix} a_5 \\ a_5 \\ a_5 \\ a_5 \\ a_5 \\ a_5 \end{bmatrix} \\
\begin{bmatrix} 0 & 0 & 0 & 0 & 0 & 0 \\ 0 & 0 & 0 & 0 & 0 & 0 \\ 0 & 0 & 0 & 0 & 0 & 0 \\ 0 & 0 & 0 & 0 & 0 & 0 \\ 0 & 0 & 0 & 0 & 0 & 0 \\ 0 & 0 & 0 & 0 & 0 & 0 \end{bmatrix} & \begin{bmatrix} x_1 & 0 & 0 & 0 & 0 & 0 \\ 0 & x_1 & 0 & 0 & 0 & 0 \\ 0 & 0 & x_1 & 0 & 0 & 0 \\ 0 & 0 & 0 & x_1 & 0 & 0 \\ 0 & 0 & 0 & 0 & x_1 & 0 \\ 0 & 0 & 0 & 0 & 0 & x_1 \end{bmatrix} & \begin{bmatrix} 0 & 0 & 0 & 0 & 0 & 0 \\ 0 & 0 & 0 & 0 & 0 & 0 \\ 0 & 0 & 0 & 0 & 0 & 0 \\ 0 & 0 & 0 & 0 & 0 & 0 \\ 0 & 0 & 0 & 0 & 0 & 0 \\ 0 & 0 & 0 & 0 & 0 & 0 \end{bmatrix} & \begin{bmatrix} x_2 & x_3 & 0 & 0 & 0 & 0 \\ 0 & x_2 & x_3 & 0 & 0 & 0 \\ 0 & 0 & x_2 & x_3 & 0 & 0 \\ 0 & 0 & 0 & x_2 & x_3 & 0 \\ 0 & 0 & 0 & 0 & x_2 & x_3 \\ x_3 & 0 & 0 & 0 & 0 & x_2 \end{bmatrix} & \begin{bmatrix} x_4 & 0 & 0 & 0 & 0 & 0 \\ 0 & x_4 & 0 & 0 & 0 & 0 \\ 0 & 0 & x_4 & 0 & 0 & 0 \\ 0 & 0 & 0 & x_4 & 0 & 0 \\ 0 & 0 & 0 & 0 & x_4 & 0 \\ 0 & 0 & 0 & 0 & 0 & x_4 \end{bmatrix} & \begin{bmatrix} x_5 \\ x_5 \\ x_5 \\ x_5 \\ x_5 \\ x_5 \end{bmatrix} \\
\begin{bmatrix} 0 & 0 & 0 & 0 & 0 & 0 \\ 0 & 0 & 0 & 0 & 0 & 0 \\ 0 & 0 & 0 & 0 & 0 & 0 \\ 0 & 0 & 0 & 0 & 0 & 0 \\ 0 & 0 & 0 & 0 & 0 & 0 \\ 0 & 0 & 0 & 0 & 0 & 0 \end{bmatrix} & \begin{bmatrix} 0 & 0 & 0 & 0 & 0 & 0 \\ 0 & 0 & 0 & 0 & 0 & 0 \\ 0 & 0 & 0 & 0 & 0 & 0 \\ 0 & 0 & 0 & 0 & 0 & 0 \\ 0 & 0 & 0 & 0 & 0 & 0 \\ 0 & 0 & 0 & 0 & 0 & 0 \end{bmatrix} & \begin{bmatrix} y_1 & 0 & 0 & 0 & 0 & 0 \\ 0 & y_1 & 0 & 0 & 0 & 0 \\ 0 & 0 & y_1 & 0 & 0 & 0 \\ 0 & 0 & 0 & y_1 & 0 & 0 \\ 0 & 0 & 0 & 0 & y_1 & 0 \\ 0 & 0 & 0 & 0 & 0 & y_1 \end{bmatrix} & \begin{bmatrix} y_2 & y_3 & 0 & 0 & 0 & 0 \\ 0 & y_2 & y_3 & 0 & 0 & 0 \\ 0 & 0 & y_2 & y_3 & 0 & 0 \\ 0 & 0 & 0 & y_2 & y_3 & 0 \\ 0 & 0 & 0 & 0 & y_2 & y_3 \\ y_3 & 0 & 0 & 0 & 0 & y_2 \end{bmatrix} & \begin{bmatrix} 0 & 0 & 0 & 0 & 0 & 0 \\ 0 & 0 & 0 & 0 & 0 & 0 \\ 0 & 0 & 0 & 0 & 0 & 0 \\ 0 & 0 & 0 & 0 & 0 & 0 \\ 0 & 0 & 0 & 0 & 0 & 0 \\ 0 & 0 & 0 & 0 & 0 & 0 \end{bmatrix} & \begin{bmatrix} 0 \\ 0 \\ 0 \\ 0 \\ 0 \\ 0 \end{bmatrix} \\
\begin{bmatrix} s_1 & 0 & 0 & 0 & 0 & s_2 \\ s_2 & s_1 & 0 & 0 & 0 & 0 \\ 0 & s_2 & s_1 & 0 & 0 & 0 \\ 0 & 0 & s_2 & s_1 & 0 & 0 \\ 0 & 0 & 0 & s_2 & s_1 & 0 \\ 0 & 0 & 0 & 0 & s_2 & s_1 \end{bmatrix} & \begin{bmatrix} s_3 & 0 & 0 & 0 & 0 & s_4 \\ s_4 & s_3 & 0 & 0 & 0 & 0 \\ 0 & s_4 & s_3 & 0 & 0 & 0 \\ 0 & 0 & s_4 & s_3 & 0 & 0 \\ 0 & 0 & 0 & s_4 & s_3 & 0 \\ 0 & 0 & 0 & 0 & s_4 & s_3 \end{bmatrix} & \begin{bmatrix} s_5 & 0 & 0 & 0 & 0 & s_6 \\ s_6 & s_5 & 0 & 0 & 0 & 0 \\ 0 & s_6 & s_5 & 0 & 0 & 0 \\ 0 & 0 & s_6 & s_5 & 0 & 0 \\ 0 & 0 & 0 & s_6 & s_5 & 0 \\ 0 & 0 & 0 & 0 & s_6 & s_5 \end{bmatrix} & \begin{bmatrix} s_7 & 0 & 0 & 0 & 0 & 0 \\ 0 & s_7 & 0 & 0 & 0 & 0 \\ 0 & 0 & s_7 & 0 & 0 & 0 \\ 0 & 0 & 0 & s_7 & 0 & 0 \\ 0 & 0 & 0 & 0 & s_7 & 0 \\ 0 & 0 & 0 & 0 & 0 & s_7 \end{bmatrix} & \begin{bmatrix} 0 & 0 & 0 & 0 & 0 & 0 \\ 0 & 0 & 0 & 0 & 0 & 0 \\ 0 & 0 & 0 & 0 & 0 & 0 \\ 0 & 0 & 0 & 0 & 0 & 0 \\ 0 & 0 & 0 & 0 & 0 & 0 \\ 0 & 0 & 0 & 0 & 0 & 0 \end{bmatrix} & \begin{bmatrix} s_8 \\ s_8 \\ s_8 \\ s_8 \\ s_8 \\ s_8 \end{bmatrix} \\
\begin{bmatrix} \alpha_1 & 0 & 0 & 0 & 0 & 0 \\ 0 & \alpha 1 & 0 & 0 & 0 & 0 \\ 0 & 0 & \alpha_1 & 0 & 0 & 0 \\ 0 & 0 & 0 & \alpha_1 & 0 & 0 \\ 0 & 0 & 0 & 0 & \alpha_1 & 0 \\ 0 & 0 & 0 & 0 & 0 & \alpha_1 \end{bmatrix} & \begin{bmatrix} \alpha_2 & 0 & 0 & 0 & 0 & 0 \\ 0 & \alpha_2 & 0 & 0 & 0 & 0 \\ 0 & 0 & \alpha_2 & 0 & 0 & 0 \\ 0 & 0 & 0 & \alpha_2 & 0 & 0 \\ 0 & 0 & 0 & 0 & \alpha_2 & 0 \\ 0 & 0 & 0 & 0 & 0 & \alpha_2 \end{bmatrix} & \begin{bmatrix} 0 & 0 & 0 & 0 & 0 & 0 \\ 0 & 0 & 0 & 0 & 0 & 0 \\ 0 & 0 & 0 & 0 & 0 & 0 \\ 0 & 0 & 0 & 0 & 0 & 0 \\ 0 & 0 & 0 & 0 & 0 & 0 \\ 0 & 0 & 0 & 0 & 0 & 0 \end{bmatrix} & \begin{bmatrix} 0 & 0 & 0 & 0 & 0 & 0 \\ 0 & 0 & 0 & 0 & 0 & 0 \\ 0 & 0 & 0 & 0 & 0 & 0 \\ 0 & 0 & 0 & 0 & 0 & 0 \\ 0 & 0 & 0 & 0 & 0 & 0 \\ 0 & 0 & 0 & 0 & 0 & 0 \end{bmatrix} & \begin{bmatrix} \alpha_3 & 0 & 0 & 0 & 0 & 0 \\ 0 & \alpha_3 & 0 & 0 & 0 & 0 \\ 0 & 0 & \alpha_3 & 0 & 0 & 0 \\ 0 & 0 & 0 & \alpha_3 & 0 & 0 \\ 0 & 0 & 0 & 0 & \alpha_3 & 0 \\ 0 & 0 & 0 & 0 & 0 & \alpha_3 \end{bmatrix} & \begin{bmatrix} \alpha_4 \\ \alpha_4 \\ \alpha_4 \\ \alpha_4 \\ \alpha_4 \\ \alpha_4 \end{bmatrix} \\
\begin{bmatrix} 0 & 0 & 0 & 0 & 0 & 0 \end{bmatrix} & \begin{bmatrix} p_1 & p_1 & p_1 & p_1 & p_1 & p_1 \end{bmatrix} & \begin{bmatrix} 0 & 0 & 0 & 0 & 0 & 0 \end{bmatrix} & \begin{bmatrix} 0 & 0 & 0 & 0 & 0 & 0 \end{bmatrix} & \begin{bmatrix} p_2 & p_2 & p_2 & p_2 & p_2 & p_2 \end{bmatrix} & \begin{bmatrix} p_3 \end{bmatrix}
\end{bmatrix}
\begin{bmatrix}
\begin{bmatrix} \bar{\phi}^1 \\ \bar{\phi}^2 \\ \bar{\phi}^3 \\ \bar{\phi}^4 \\ \bar{\phi}^5 \\ \bar{\phi}^6 \end{bmatrix} \\
\begin{bmatrix} \tilde{\phi}_x^1 \\ \tilde{\phi}_x^2 \\ \tilde{\phi}_x^3 \\ \tilde{\phi}_x^4 \\ \tilde{\phi}_x^5 \\ \tilde{\phi}_x^6 \end{bmatrix} \\
\begin{bmatrix} \tilde{\phi}_y^1 \\ \tilde{\phi}_y^2 \\ \tilde{\phi}_y^3 \\ \tilde{\phi}_y^4 \\ \tilde{\phi}_y^5 \\ \tilde{\phi}_y^6 \end{bmatrix} \\
\begin{bmatrix} \bar{\phi}_s^1 \\ \bar{\phi}_s^2 \\ \bar{\phi}_s^3 \\ \bar{\phi}_s^4 \\ \bar{\phi}_s^5 \\ \bar{\phi}_s^6 \end{bmatrix} \\
\begin{bmatrix} \bar{J}_x^{1,o} \\ \bar{J}_x^{2,o} \\ \bar{J}_x^{3,o} \\ \bar{J}_x^{4,o} \\ \bar{J}_x^{5,o} \\ \bar{J}_x^{6,o} \end{bmatrix} \\
\begin{bmatrix} \phi_c \end{bmatrix}
\end{bmatrix}
=
\begin{bmatrix}
\begin{bmatrix} \bar{q}^1 \\ \bar{q}^2 \\ \bar{q}^3 \\ \bar{q}^4 \\ \bar{q}^5 \\ \bar{q}^6 \end{bmatrix} \\
\begin{bmatrix} \tilde{q}_x^1 \\ \tilde{q}_x^2 \\ \tilde{q}_x^3 \\ \tilde{q}_x^4 \\ \tilde{q}_x^5 \\ \tilde{q}_x^6 \end{bmatrix} \\
\begin{bmatrix} \tilde{q}_y^1 \\ \tilde{q}_y^2 \\ \tilde{q}_y^3 \\ \tilde{q}_y^4 \\ \tilde{q}_y^5 \\ \tilde{q}_y^6 \end{bmatrix} \\
\begin{bmatrix} \bar{q}_s^1 \\ \bar{q}_s^2 \\ \bar{q}_s^3 \\ \bar{q}_s^4 \\ \bar{q}_s^5 \\ \bar{q}_s^6 \end{bmatrix} \\
\begin{bmatrix} q_j^1 \\ q_j^2 \\ q_j^3 \\ q_j^4 \\ q_j^5 \\ q_j^6 \end{bmatrix} \\
\begin{bmatrix} q_c \end{bmatrix}
\end{bmatrix}
\tag{3.2-1}
$$

where

$$
a_1 = x_1 = y_1 = \begin{bmatrix} 80\dfrac{D_1}{h^2} + \Sigma_{r1} - \dfrac{1}{k_{eff}}\nu\Sigma_{f1} & -\dfrac{1}{k_{eff}}\nu\Sigma_{f2} \\ -\Sigma_{s21} & 80\dfrac{D_2}{h^2} + \Sigma_{r2} \end{bmatrix}, \quad a_2 = a_3 = -\frac{32}{h^2}\begin{bmatrix} D_1 & 0 \\ 0 & D_2 \end{bmatrix},
$$

$$
a_4 = 2a_3, \quad a_5 = -\frac{1}{6}a_2, \quad \bar{q}^m = \bar{S}_z^m - a_4\bar{J}_x^{m,i} - a_5\left(\phi^m + \phi^{m+1}\right),
$$

$$x_2 = x_3 = -\frac{1}{12}a_2, \quad x_4 = \frac{1}{3}a_2, \quad x_5 = -\frac{1}{18}a_2, \quad \tilde{q}_x^n = \tilde{S}_{zx}^m - x_4\bar{J}_x^{n,i} + \frac{1}{2}x_5\left(\phi^n + \phi^{n+1}\right),$$

$$y_2 = \frac{1}{4}a_2, \quad y_3 = -y_2, \quad \tilde{q}_y^m = \tilde{S}_{zy}^m + \frac{1}{3}y_2\left(\phi^m - \phi^{m+1}\right),$$

$$s_1 = s_2 = -10\mathbf{I}, \quad s_3 = s_4 = s_6 = -3s_1, \quad s_5 = -s_6, \quad s_7 = -\frac{12}{5}s_1, \quad s_8 = \frac{1}{10}s_1,$$

$$\bar{q}_s^m = -s_8\left(\phi^{m-1} + \phi^m + \phi^{m+1}\right),$$

$$\alpha_1 = -\frac{20\sqrt{3}}{3h}\begin{bmatrix} D_1 & 0 \\ 0 & D_2 \end{bmatrix}, \quad \alpha_2 = 6\alpha_1, \quad \alpha_3 = \mathbf{I} - \frac{12}{5}\alpha_1, \quad \alpha_4 = \frac{1}{10}\alpha_1,$$

$$\bar{q}_j^m = -\frac{1}{2}\alpha_4\left(\phi^m + \phi^{m+1}\right) + \left(\mathbf{I} + \frac{12}{5}\alpha_1\right)\bar{J}_x^{m,i},$$

$$p_1 = 15\mathbf{I}, \quad p_2 = -2\mathbf{I}, \quad p_3 = 6\mathbf{I}, \qquad q_c = -p_2\sum_{m=1}^{6}\bar{J}_x^{m,i},$$

$$\bar{\phi}^m = \begin{bmatrix} \bar{\phi}_1^m \\ \bar{\phi}_2^m \end{bmatrix}, \quad \tilde{\phi}_x^m = \begin{bmatrix} \tilde{\phi}_{1x}^m \\ \tilde{\phi}_{2x}^m \end{bmatrix}, \quad \tilde{\phi}_y^m = \begin{bmatrix} \tilde{\phi}_{1y}^m \\ \tilde{\phi}_{2y}^m \end{bmatrix}, \quad \bar{\phi}_s^m = \begin{bmatrix} \bar{\phi}_{1s}^m \\ \bar{\phi}_{2s}^m \end{bmatrix}, \quad \bar{J}_x^{m,o} = \begin{bmatrix} \bar{J}_{1x}^{m,o} \\ \bar{J}_{2x}^{m,o} \end{bmatrix}, \quad \phi_c = \begin{bmatrix} \phi_{1c} \\ \phi_{2c} \end{bmatrix},$$

$$\bar{J}_x^{m,i} = \begin{bmatrix} \bar{J}_{1x}^{m,i} \\ \bar{J}_{2x}^{m,i} \end{bmatrix}, \quad \phi^m = \begin{bmatrix} \phi_1^m \\ \phi_2^m \end{bmatrix}, \quad \bar{S}_z^m = \begin{bmatrix} \bar{S}_{1z}^m \\ \bar{S}_{2z}^m \end{bmatrix}, \quad \tilde{S}_{zx}^m = \begin{bmatrix} \tilde{S}_{1zx}^m \\ \tilde{S}_{2zx}^m \end{bmatrix}, \quad \bar{S}_{zy}^m = \begin{bmatrix} \bar{S}_{1zy}^m \\ \bar{S}_{2zy}^m \end{bmatrix}.$$

m=1,...,6, triangular node number.

The above linear system can be solved directly by a block Gaussian Elimination scheme provided the aforementioned boundary conditions.

3.3 Point Flux Calculation at Hexagon Corners

In order to determine the corner point fluxes from the CMFD solution, it is required to update the moments and surface fluxes according to Eq. (3.1-17). Since it is not straightforward to update the moments based on the node average flux information obtained

from a CMFD solution, an alternative corner flux determination method is employed in the TPEN method applied within the CMFD framework. The following section provides the details of the alternative [5] that uses a 13 term polynomial expansion and corner point balance conditions. Under this scheme employed to determine the corner point fluxes of the hexagon, Eq. (3.1-17) is used just for the determination of the center point flux of the hexagon.

For the evaluation of point fluxes at hexagon corners, the intra-nodal flux is approximated as:

$$\begin{aligned}\phi_g^m(x,y) = C_0^m &+ A_{gz}^m \xi_{10}(x) + B_{gx}^m \xi_{20}(x) + C_{gx}^m \xi_{01}(y) + D_{gx}^m \xi_{02}(y) \\ &+ A_{gu}^m \xi_{10}(u) + B_{gu}^m \xi_{20}(u) + C_{gu}^m \xi_{01}(v) + D_{gu}^m \xi_{02}(v) \\ &+ A_{gp}^m \xi_{10}(p) + B_{gp}^m \xi_{20}(p) + C_{gp}^m \xi_{01}(q) + D_{gp}^m \xi_{02}(q)\end{aligned} \tag{3.3-1}$$

where $\xi_{10}(t) = t^3 + t$, $\xi_{20}(t) = t^4 + t^2$, $\xi_{01}(t) = t^3 - t$, $\xi_{02}(t) = t^4 - t^2$.

The 13 coefficients are easily determined by using 1 assembly average flux, 6 surface fluxes and 6 corner point fluxes.

In order to determine the corner point fluxes, the same leakage balance method as the one used for the determination of the center point flux is used. Fig.3-5 shows 3 hexagonal nodes surrounding a corner point and corresponding unknowns. The leakage balance equation for center point flux of Fig.3-5 is:

$$\sum_{m=1}^{3} L_g^m = 0. \tag{3.3-2}$$

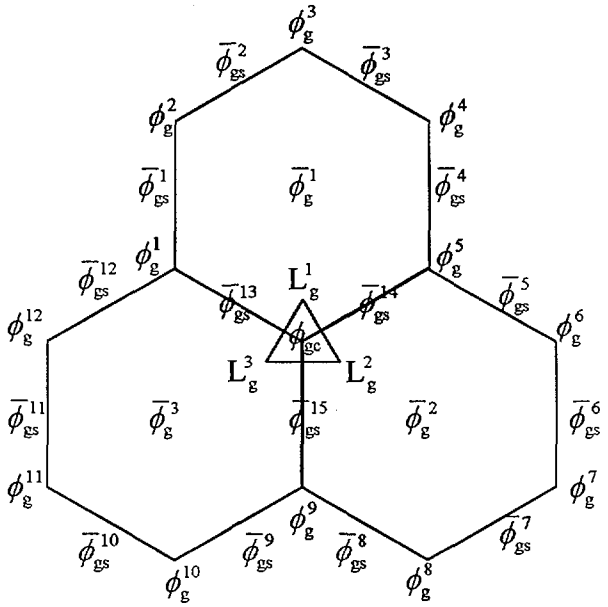

Figure 3-5. Three hexagonal assemblies surrounding one corner point

The net neutron leakage from nodes 1,2 and 3 at the corner can be expressed in terms of nodal unknowns defined in Fig.3-5. Inserting those expressions to Eq. (3.3-2), one can obtain leakage balance equation as:

$$\begin{aligned}&\left(D_g^1+D_g^2+D_g^3\right)\phi_{gc}+w_1\left\{\left(D_g^1+D_g^3\right)\phi_g^1+\left(D_g^1+D_g^2\right)\phi_g^5+\left(D_g^2+D_g^3\right)\phi_g^9\right\}\\&+w_2\left\{D_g^1\left(\phi_g^2+\phi_g^4\right)+D_g^2\left(\phi_g^6+\phi_g^8\right)+D_g^3\left(\phi_g^{10}+\phi_g^{12}\right)\right\}+w_3\left(D_g^1\phi_g^3+D_g^2\phi_g^7+D_g^3\phi_g^{11}\right)=q_{gc}\end{aligned} \tag{3.3-3}$$

where

$$\begin{aligned}q_{gc}=&\,w_4\left\{\left(D_g^1+D_g^3\right)\bar{\phi}_{gx}^{13}+\left(D_g^1+D_g^2\right)\bar{\phi}_{gx}^{14}+\left(D_g^2+D_g^3\right)\bar{\phi}_{gx}^{15}\right\}\\&+w_5\left\{D_g^1\left(\bar{\phi}_{gx}^1+\bar{\phi}_{gx}^4\right)+D_g^2\left(\bar{\phi}_{gx}^5+\bar{\phi}_{gx}^8\right)+D_g^3\left(\bar{\phi}_{gx}^9+\bar{\phi}_{gx}^{12}\right)\right\}\\&+w_6\left\{D_g^1\left(\bar{\phi}_{gx}^2+\bar{\phi}_{gx}^3\right)+D_g^2\left(\bar{\phi}_{gx}^6+\bar{\phi}_{gx}^7\right)+D_g^3\left(\bar{\phi}_{gx}^{10}+\bar{\phi}_{gx}^{11}\right)\right\}+w_7\left(D_g^1\bar{\phi}_x^1+D_g^2\bar{\phi}_x^2+D_g^3\bar{\phi}_x^3\right)\end{aligned}$$

$$w_1=\frac{342}{1141},\quad w_2=-\frac{74}{2119},\quad w_3=\frac{2187}{74165},\quad w_4=\frac{648}{815},\quad w_5=\frac{672}{10595},$$

$$w_6=-\frac{120}{14833},\quad w_7=-\frac{10512}{74165}.$$

In Eq.(3.3-3), the source term for the corner flux is determined by the node average fluxes and surface fluxes which are already known from the CMFD solution. Therefore, the linear system for corner fluxes can be established easily from Eq.(3.3-3) applied to all the corners. This linear system for point fluxes is solved by the plain Gauss-Seidel iteration scheme since it is strongly diagonally dominant.

3.4 Axial Leakage Source Approximation

The three-dimensional neutron diffusion equation can be reduced to a two-dimensional one by integrating over the axial direction as:

$$
\begin{aligned}
&-D_g^m\left(\frac{\partial^2}{\partial x^2}+\frac{\partial^2}{\partial y^2}\right)\phi_g^m(x,y)+\Sigma_{rg}^m\phi_g^m(x,y) \\
&\qquad=\frac{\chi_g}{k_{eff}}\sum_{g'}\nu\Sigma_{fg'}^m\phi_{g'}^m(x,y)+\sum_{g'}\Sigma_{sgg'}^m\phi_{g'}^m(x,y)+S_{gz}^m(x,y),
\end{aligned}
\tag{3.4-1}
$$

where

$$
\begin{aligned}
\phi_g^m(x,y)&=\frac{1}{h_z^m}\int\phi_g^m(x,y,z)\,dz, \\
S_{gz}^m(x,y)&=-\frac{1}{h_z^m}\int-D_g^m\frac{\partial^2}{\partial z^2}\phi_g^m(x,y,z)\,dz \\
&=-\frac{1}{h_z^m}\left(J_{gz}^{m,T}(x,y)-J_{gz}^{m,B}(x,y)\right).
\end{aligned}
$$

The superscript 'T' and 'B' denote top and bottom surface of node m repectively, and S_{gz}^m is the axial leakage source which comes from the axial leakage term. Eq.(3.4-1) means that the

radial distribution of the axial leakage source should be pre-determined to obtain a radial solution. In the MASTER code, a NEM solver generates the surface average axial currents that are fed into the TPEN solver as the axial leakage source. The radial shape of the axial leakage source is considered in the following.

Fig.3-6 shows the node average axial leakages for one center and 6 neighboring hexagons. The axial leakage sources is defined as:

$$\bar{S}_{gz}^{m} = -\frac{1}{h_z^m}\left(\bar{J}_{gz}^{m,T} - \bar{J}_{gz}^{m,B}\right). \tag{3.4-2}$$

Using the 7 node average axial leakages shown in Fig. 3-6, the radial dependence of the axial leakage within the central hexagon can be approximated employing a two-dimensional polynomial consisting of 7 independent terms as:

$$S_{gz}(x,y) = d_{g0} + d_{g1}x + d_{g2}y + d_{g3}x^2 + d_{g4}u^2 + d_{g5}p^2 + d_{g6}xup. \tag{3.4-3}$$

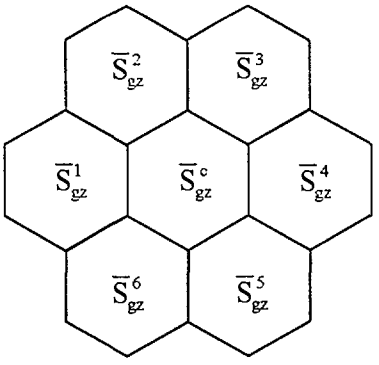

Figure 3-6. Notations for Axial Sources near Center Hexagon

The 7 coefficients of Eq.(3.4-3) can be determined by imposing 7 node average axial leakage constraints.

The TPEN solver requires three kinds of axial leakage source parameters on a triangle: triangular averaged axial sources, and x- and y- source moments. Fig. 3-7 shows these axial leakage source parameters of the 6 triangles of the central hexagon which are defined as:

$$\begin{aligned}
\bar{S}_{gz}^{c,n} &= \frac{1}{A^n}\int_{A^n} S_{gz}(x,y)\,dA \ , \\
\tilde{S}_{gzx}^{c,n} &= \frac{2}{\sqrt{3}h}\frac{1}{A^n}\int_{A^n} xS_{gz}(x,y)\,dA \ , \\
\tilde{S}_{gzy}^{c,n} &= \frac{2}{h}\frac{1}{A^n}\int_{A^n} yS_{gz}(x,y)\,dA \ .
\end{aligned} \tag{3.4-4}$$

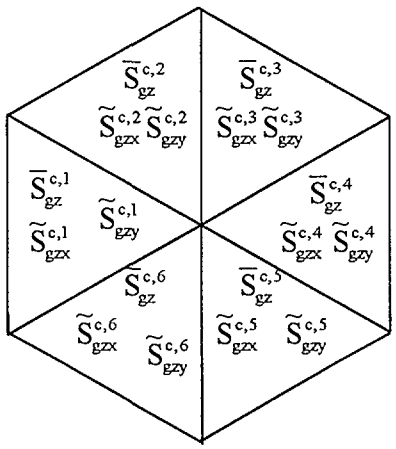

Figure 3-7. Triangular Axial Leakage Source Parameters

By inserting Eq.(3.4-3) to (3.4-4), one can obtain axial sources which are expressed by 7 hexagon averaged axial leakage sources of Fig.3-6. For example, the axial sources of the 1st triangle of center hexagon is:

$$\bar{S}_{gz}^{c,l} = w_1 S_{gz}^{c} + w_2 S_{gz}^{l} + w_3 \left(S_{gz}^{2} + S_{gz}^{6}\right) + w_4 \left(S_{gz}^{3} + S_{gz}^{5}\right) + w_5 S_{gz}^{4},$$

$$\tilde{S}_{gzx}^{c,l} = w_{x1} S_{gz}^{c} + w_{x2} S_{gz}^{l} + w_{x3} \left(S_{gz}^{2} + S_{gz}^{6}\right) + w_{x4} \left(S_{gz}^{3} + S_{gz}^{5}\right) + w_{x5} S_{gz}^{4}, \qquad (3.4\text{-}5)$$

$$\tilde{S}_{gzy}^{c,l} = w_{y1} \left(S_{gz}^{2} - S_{gz}^{6}\right) + w_{y2} \left(S_{gz}^{3} - S_{gz}^{5}\right).$$

where

$$w_1 = 1, \quad w_2 = \frac{83}{540}, \quad w_3 = \frac{17}{540}, \quad w_4 = -\frac{37}{540}, \quad w_5 = -\frac{43}{540},$$

$$w_{x1} = -\frac{1}{54}, \quad w_{x2} = \frac{59}{3240}, \quad w_{x3} = \frac{7}{1620}, \quad w_{x4} = -\frac{1}{324}, \quad w_{x5} = -\frac{7}{3240},$$

$$w_{y1} = \frac{1}{40}, \quad w_{y2} = \frac{1}{360}.$$

3.5 Adjoint Calculation and Core Reactivity

Since the converged solution of the forward problem includes the converged CMFD coefficient matrix, the adjoint problem within the nonlinear nodal method can be easily formulated by taking the transpose of the final CMFD coefficient matrix after the forward solution is obtained. The adjoint CMFD system can then be solved using the same solution method as for the forward problem, or by using the same Krylov and the Wielandt shift methods as the forward problem.

At a time point during a transient, the dynamic reactivity is defined as:

$$\rho = \frac{\langle \phi_0^*, A\phi \rangle}{\langle \phi_0^*, F\phi \rangle}. \qquad (3.5\text{-}1)$$

where **A** is the net production operator which is defined as **A** =**F** -**M**. Note that this definition gives ρ=0 if the steady-state values of the operators and the flux vector are used.

4. Implementation and Control Logic

A non-linear TPEN method is implemented to the MASTER code as a new solver for hexagonal core design and analysis. The calculation flow logic control involves a global coordination of these modular solutions as well as local controls in each calculation module. Since any transient should starts with an initial steady-state that is to be solved as an eigenvalue problem, the description of the calculation flow starts with the eigenvalue calculation. In the following the description is given in the order of actual calculation flow.

4.1 Eigenvalue Calculation Flow Control

Figure 4-1 shows brief view on how a non-linear TPEN solver works with MASTER. The MASTER code generates the cross sections from thermal/hydraulic calculation and manages all processes, and the non-linear TPEN method solves a two-group diffusion equation for hexagonal core. The MASTER code and the TPEN solver transfer key data to each other iteratively until solution converged .

The non-linear TPEN solver consists of two major modules, CMFD and nodal solver, and solves hexagonal core from the cross section transferred from the MASTER code. The CMFD solver performs a Wielandt eigenvalue shift outer iteration with updated D-hat and calls nodal solver to update D-hat if it meets convergence criteria. Nodal solver consists of three parts, point solver which calculates corner fluxes from corner point balance equation, TPEN solver and NEM axial solver. Nodal solver sweeps all the hexagonal nodes two times in

forward and backward direction.

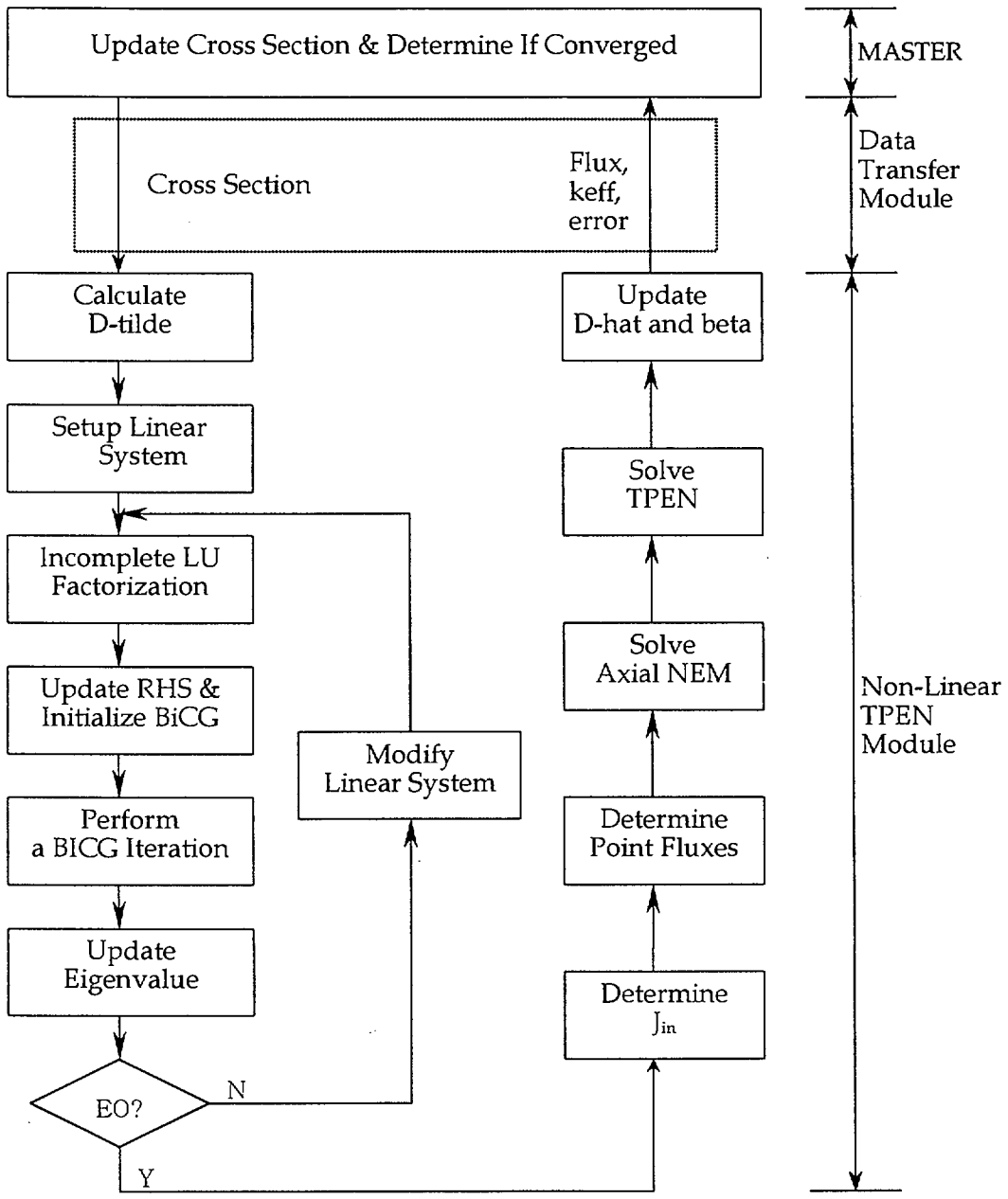

Figure 4-1. Eigenvalue Calculation Logic

4.1.1 Initialize BiCGSTAB Parameters

Under the framework of the Wielandt eigenvalue shift, the left hand side (LHS) of the CMFD linear system contains fission cross section devided by eigenvalue shifted, which means the diagonal part of CMFD linear system changes with eigenvalue converging. Therefore the initial residual vector and other vectors and scalars needed to be reset to initialize the BiCGSTAB algorithm.

4.1.2 Inner Iteration

The inner iteration to solve the linear system for a given partial fission source is performed by BiCG stabilized algorithm with incomplete LU factorization which shows a fast convergence characteristic. Therefore the number of inner-iteration is fixed to 2 without checking any convergence parameter.

4.1.3 Outer Iteration

The outer iteration driver controls the updates of eigenvalue with fixed group constants and nodal coupling coefficients. The eigenvalue update is performed by the Wielandt eigenvalue shift method. The outer iteration routine exits if it meet sone of the following criteria:

1) number of iterations, *i>noutmax?*, or
2) sufficient error reduction, $\frac{\| r_i \|}{\| r_0 \|} < \varepsilon_{ERF}$.

4.1.4 Determination of Incoming Partial Current from Node Average Fluxes

Once the node-average flux distribution is known, the net current at every nodal surface can be obtained using Eq. (2.1-1). If the surface fluxes are also known, the incoming partial currents can be determined from the two as follows:

$$J_{in} = \frac{1}{4}\phi + \frac{1}{2}J_{net}. \tag{4.1-1}$$

Now the problem is how to determine the surface fluxes from the node-average fluxes. This is achieved a similar relation to Eq. (2.1-1) for the surface flux as follows:

$$\phi_s = \alpha\phi_R + (1-\alpha)\phi_L + \beta(\phi_R + \phi_L). \tag{4.1-2}$$

The α factor in the above equation relates the surface flux with the two node-average fluxes in the finite difference approximation while the β factor represents a correction term that is obtainable from a nodal calculation just like D-hat's. As long as the β factor is calculated during the TPEN updates and stored, the surface fluxes can be accurately determined from the node-average fluxes.

4.1.5 Corner Point Flux Calculation

In the TPEN calculation, in addition to six incoming partial currents defined at the surfaces of a hexagon, six corner point fluxes are required as the boundary conditions for the TPEN

solver to complete the triangular polynomial expansion uniquely. Since the corner point fluxes as well as the incoming partial currents are not the unknowns directly determined by the CMFD calculation (only node average fluxes are unknowns), there must be supplemental methods to determine these boundary conditions from the node-average flux distribution. Section 3.3 detailed the method of corner point flux calculation. Since surface fluxes and node average fluxes are known from the CMFD results, it is possible to construct the CPB condition for each corner point from the Eq. (3.3.3). The set of CPB equations then constitutes a CPB linear system that contains point fluxes as the unknowns and the surface and node average fluxes as the RHS terms. This linear system is very diagonally dominant because the corner point flux is determined by the flux shapes of only a small neighboring region. Thus the linear system is solved by the plain Gauss-Seidel sweep and even only a few iterations suffice. Note that the CPB linear system is set up separately for each plane and each energy group, and thus the size of the linear system is not large.

4.1.6 One-Node Axial NEM Solution

Since the axial leakage is considered as source in the TPEN formulation, the axial leakage and its functional dependence over the radial domain are also required as the prerequisite to the TPEN solver. The axial intranodal flux distribution is solved by the NEM method with the radial leakage as the transverse leakage source. The NEM calculation is performed for each one-node with the incoming current boundary conditions specified at both lower and upper boundaries. The resulting outgoing current is used to update the net axial currents that determine the hexagon averaged axial leakages.

4.1.7 One-Node TPEN Solution

The purpose of the TPEN calculation is to update D-hat to be used in Eq. (2.1-1). TPEN calculates net neutron currents based on the flux distribution determined by a CMFD calculation and then adjusts D-hat's to retrieve the newly calculated net currents. The primary results of the TPEN calculation for a node are the outgoing currents and the node-average fluxes. The new outgoing current is then used to update the net current.

Once the boundary conditions and the axial leakage are determined, the TPEN calculation begins. However, one additional step is required to obtain the functional dependence of the axial leakage over the radial domain. Section 3.4 detailed the method to get a radial dependence of axial leakage. TPEN solver actually finds an intranodal flux expansion for each triangle within a hexagon in terms of a two-dimensional third order polynomial consisting of 9 mutually independent terms. The process of determining the polynomial coefficients is detailed in Sections 3.1 and 3.2.

The one-node TPEN nodal solution is performed for all the nodes by the forward sweep scheme employing a three-color (red-green-blue) checkerboard type radial node-ordering scheme. In this type of sweep, the one-node calculation is performed for all the nodes belonging to a color, and then moves to another colored nodes. The newly determined outgoing currents for one-colored nodes are then used as the incoming partial currents of the other-colored nodes so that a Gauss-Seidel type update of incoming partial current is achieved in the TPEN forward sweep. Once the forward sweep is completed, a backward

sweep is also performed so that the resulting incoming current update scheme becomes symmetric Gauss-Seidel. This dual sweep scheme was chosen to achieve a stable convergence behavior.

After the dual sweeps are completed, the net currents are updated and also the D-hat's accordingly. This completes the TPEN nodal updates and the next CMFD calculation is to be performed. In the following, details of each TPEN module that were not described in the above are provided.

4.1.8 Nodal Coupling Parameter Update

Once the TPEN solution is obtained, the outgoing partial current as well as the surface fluxes can be determined. In terms of the newly determined all the outgoing partial current, the net current is obtained as the difference of the two outgoing partial currents (positive and negative directions) defined at a surface and D-hat's obtained to force that the net current be obtained by Eq. (2.1-1). Namely,

$$\hat{D} = \frac{J^r_{out}\big|_L - J^l_{out}\big|_R - \tilde{D}(\phi_R - \phi_L)}{\phi_R + \phi_L} \tag{4.1-3}$$

Similarly the β factors to be used in Eq. (4.1-2) are calculated for each surface from the surface fluxes.

4.2 Transient Calculation Flow Control

The transient calculation flow given in Figure 4-2 is somewhat similar to the steady-state one in that the CMFD and nodal updates are alternatively performed and the same calculation modules are used. The major difference lies in that the transient calculation solves a fixed source problem and thus there is no eigenvalue update part and also the fixed source must be considered in the TPEN solution. In the following, transient specific calculation control logics are described.

4.2.1 Formulation of Transient Fixed Source Problem

Temporal discretization of the time-dependent neutron balance equation yields a transient fixed source problem. The resulting CMFD linear system for the transient fixed source problem can be represented in the operator form as:

$$\left(\mathrm{M}+\frac{1+\mathrm{w}\Delta\mathrm{t}}{\mathrm{v}\Delta\mathrm{t}}\mathrm{I}-\left(1-\sum_{\mathrm{i}}\beta_{\mathrm{i}}\frac{\mathrm{w}+\lambda_{\mathrm{i}}\mathrm{e}^{-(\mathrm{w}+\lambda_{\mathrm{i}})\Delta\mathrm{t}}}{\mathrm{w}+\lambda_{\mathrm{i}}}\right)\mathrm{F}\right)\phi_{\mathrm{n}}=\frac{\mathrm{e}^{\mathrm{w}\Delta\mathrm{t}}}{\mathrm{v}\Delta\mathrm{t}}\phi_{\mathrm{n-1}}+\mathrm{S}_{\mathrm{d}}^{\mathrm{n}} \qquad (4.2\text{-}1)$$

where β, $\mathrm{S}_{\mathrm{d}}^{\mathrm{n}}$, and w represent the fraction, source, and current contribution fraction of delayed neutrons.

4.2.2 Outer Iteration

The outer iteration routine exits if it meets one of the following criteria:

1) Number of iterations, *i>noutmax?*, or

2) Sufficient error reduction, $\frac{\| \mathbf{r}_i \|}{\| \mathbf{r}_0 \|} < \varepsilon_{\text{ERF}}$.

4.2.3 Nodal Update Control

In non-linear nodal method, the nodal update needs not be updated at every time step. Rather the nodal update is invoked only when there are substantial changes in the total cross sections. The *NU* checkup in Figure 4-2 incorporates this conditional nodal update logic. The criterion for the conditional nodal update is given by the user input data.

4.2.4 Effective Source for Nodal Calculations

During the transient calculation, the nodal solver can in principle solve the continuous of Eq. (4.2-1). In such case, however, an accurate representation of the spatial dependence of the fixed source term is required. Since it is nontrivial to obtain such functional dependence, an alternate form of Eq. (4.2-1) is solved in the TPEN module, that has the non steady-state terms such as $\frac{1}{v\Delta t}$ only on the right-hand side. Bringing such terms from the LHS makes the magnitude of the source term smaller so that the error in spatial dependence of the source term has less impact on the solution. This scheme also help achieve a constant solution for a null transient because the LHS remains the same as the steady-state calculation while the RHS becomes nil. More specifically, the effective source to be used in the nodal solver appears as:

$$S_{eff} = S_d^n + \frac{1}{v\Delta t}(\phi_{n-1} - \phi_n) - (1 - \beta_p)F\phi_n . \qquad (4.2\text{-}2)$$

Since the effective source term includes the current time step's flux, Eq. (4.2-2) has to be iteratively updated. Once the node-average effective source terms are obtained, they are added to the transverse leakage term and thus the same spatial representation as the transverse leakage is used for the effective source.

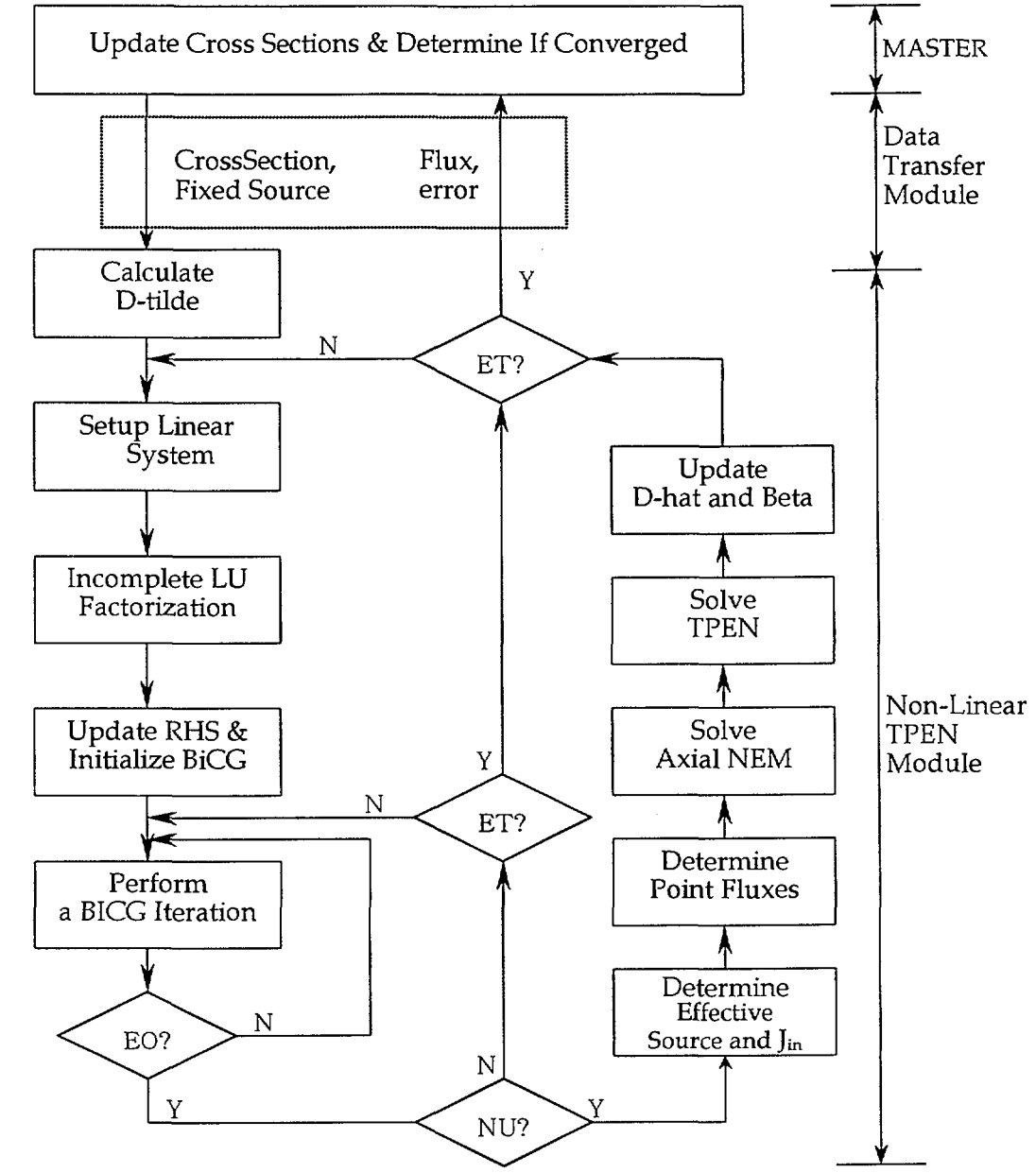

EO= Exit Outer Update, NU=Nodal Update, ET = Exit Non-Linear TPEN.

Figure 4-2. Transient Calculation Logic

5. Computational Results

In order to examine the solution accuracy of the TPEN hexagonal solution, several eigenvalue benchmark problems[6] and two transient problems, i.e., a realistic VVER1000 rod ejection benchmark problem[7-8] and VVER440 rod ejection benchmark problem, were solved and compared with respective references.

5.1 Eigenvalue Calculation Results

Table 5-1 summarizes the eigenvalue and assembly power errors for the eigenvalue benchmark problems. As shown in the table, the maximum eigenvalue error is 15 pcm and the maximum power distribution error is less than 1%, which confirm that the solution accuracy of the TPEN solver is excellent. It also provides the computing times for the two 3D benchmark problems. The run time for a large hexagonal full core consisting of 421 hexagonal nodes and 12 planes (total 5052 nodes) is 4.5 seconds on a 733 Mhz Pentium-III PC. This indicates the execution time is also very fast comparing with the original hexagonal core analysis method, i.e, the AFEN/NEM hybrid method[5] accelerated using coarse-mesh rebalancing(CMR) method. The radial power distribution errors shown in Figures 5-1 and 5-2 for the VVER1000 and VVER440 3D benchmark problems indicate very good results as well irrespective of the assembly locations.

Table 5-1. TPEN Solution Accuracy for Hexagonal Eigenvalue Benchmark Problems

Problems	Eigenvalue errors (pcm)	Assemblywise Power Errors(%)			Computing Time(sec)*	
		Max.	Avg.	RMS	TPEN	AFEN
IAEA with Reflector(α =0.5)	+15	0.41	0.20	0.21		
(α =0.125)	+10	0.18	0.10	0.10		
IAEA w/o Reflector(α =0.5)	+2	0.12	0.03	0.02		
(α =0.125)	-4	0.44	0.06	0.08		
VVER-1000 2D (α =0.5)	-15	0.98	0.29	0.30		
(α =0.125)	-15	0.90	0.20	0.23		
VVER-440 2D	+0	0.36	0.14	0.16		
Large HWR 2D	+2	0.20	0.05	0.07		
VVER-1000 3D	-12	0.99	0.20	0.23	1.7	4.1
VVER-440 3D	+4	0.37	0.15	0.17	4.5	13.8

*Computing Time on 733 MHz PENTIUM-III

```
TPEN                0.5222
REFERENCE           0.5237
ERROR(%)            -0.29

                  0.9744  0.6903
                  0.9759  0.6905
                   -0.15   -0.03

              0.8655  0.8209  0.7100
              0.8667  0.8193  0.7104
               -0.14    0.20   -0.06

          1.2007  0.8960  0.9799  0.6489
          1.1989  0.8963  0.9833  0.6503
            0.15   -0.03   -0.35   -0.22

      1.4941  1.1554  0.6548  0.6999  0.5095
      1.4902  1.1551  0.6551  0.7000  0.5114
        0.26    0.03   -0.05   -0.01   -0.37

  1.7905  1.4916  1.2042  1.1144  0.6135  0.3697
  1.7921  1.4880  1.2027  1.1186  0.6145  0.3734
   -0.09    0.24    0.12   -0.38   -0.16   -0.99

0.9394  1.4151  1.5916  1.8557  1.1443  0.8520  0.7448
0.9391  1.4124  1.5863  1.8583  1.1423  0.8505  0.7446
  0.03    0.19    0.33   -0.14    0.18    0.18    0.03

                    Max. Error    0.99 %
                    Avg. Error    0.20 %
                    RMS Error     0.23 %
```

Figure 5-1. Radial Power Distribution Errors for the VVER-1000 3D Benchmark Problem

TPEN							1.0412	0.8701	
REFERENCE							1.0399	0.8682	
ERROR(%)							0.12	0.22	
					1.1200	1.1599	1.2431	0.7696	
					1.1199	1.1588	1.2416	0.7681	
					0.01	0.09	0.12	0.19	
				1.0093	0.8312	0.8945	0.9160	1.1651	
				1.0105	0.8317	0.8944	0.9152	1.1618	
				-0.11	-0.06	0.01	0.09	0.28	
			1.0246	0.7989	0.8028	1.0699	1.1658	1.4136	1.0239
			1.0268	0.8006	0.8040	1.0705	1.1651	1.4121	1.0218
			-0.22	-0.21	-0.15	-0.06	0.06	0.11	0.21
		0.9693	0.8055	1.0274	1.0099	0.9881	0.8434	0.9509	1.3361	0.8069
		0.9721	0.8078	1.0298	1.0117	0.9895	0.8438	0.9505	1.3344	0.8056
		-0.29	-0.29	-0.24	-0.18	-0.14	-0.05	0.04	0.12	0.16
0.5975	0.6985	0.9903	1.0326	0.8079	0.7668	0.7127	1.1195	1.4778	0.9268	
0.5993	0.7011	0.9932	1.0351	0.8098	0.7684	0.7126	1.1193	1.4763	0.9242	
-0.31	-0.37	-0.29	-0.24	-0.23	-0.21	0.00	0.02	0.10	0.28	

Max. Error	0.37 %
Avg. Error	0.15 %
RMS Error	0.17 %

Figure 5-2. Radial Power Errors for the VVER440 3D Benchmark Problem

5.2 VVER1000 Rod Ejection Benchmark Result

This benchmark solves a 3-rod ejection problem out of a hexagonal core consisting of 163 fuel assemblies. The initial power of the core is 10% of nominal rated power and the transient core power reaches upto about 90% after the rod ejection. The cross sections, kinetics parameters, boundary conditions, T/H inlet conditions and fuel property data are all given and thus the problem is self-sustaining.

The steady-state critical boron concentration search at the initial 10 % power yields 1374 ppm. This value is a little bit off from 1405 ppm given in the report. However, about 30 ppm is not considered significant considering that there are many modeling discrepancies between the two codes.

The transient core power behaviors obtained for the rod ejection are given in Figure 5-3 and compared with the results of SAS-DIF3DK[9] and TENAR[10]. Two results were obtained from TPEN transient calculations, one using 2 msec time step size and the other using 10 msec as the primary time step size for the rapid power change region. Figure 5-3 shows that the solution accuracy of the two cases from TPEN calculation are essentially the same. The TPEN transient core power behaviors around the peak power range are very similar with TENAR but about 10 % higher than SAS-DIF3DK. The core powers of TPEN at the end of core transient are more similar with SAS-DIF3DK than TENAR. The computing time data for each MASTER solution module is given in Table 5-2 for the 10 msec case. The total computation time is about 50 seconds for the 5 sec transient and the spread of the computing time of the three major solution modules is quite reasonable.

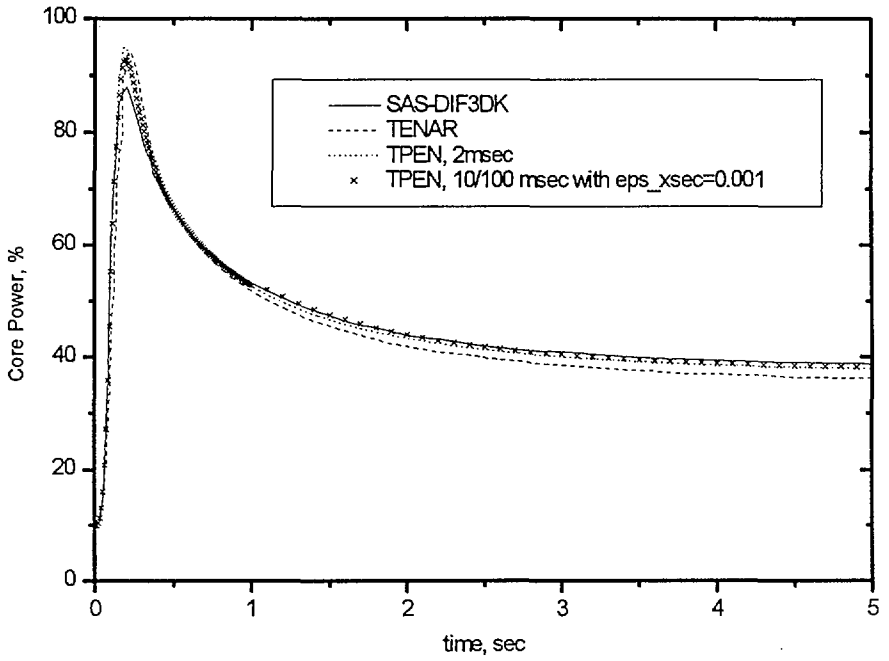

Figure 5-3. Transient Core Powers for the VVER1000 Rod Ejection Benchmark

Table 5-2. Computing Time Breakups for the 5 Sec VVER1000 Rod Ejection Transient (733 MHz Pentium-III PC, seconds)

CMFD	20.8 (42.1%)
Nodal	10.2 (20.6%)
T/H	12.1 (24.5%)
Miscellaneous	6.3 (12.8%)
Total	49.4 (100.0%)

5.3 VVER440 Rod Ejection Benchmark Result

This benchmark problem is available at the following web site:

http://www.kfki.hu/~aekihp/AER_home/bench_book

This three-dimensional dynamic benchmark(Test ID: AER-DYN-003) in hexagonal core geometry concerns a control rod ejection accident in a VVER-440 core. It includes the modelling of thermal hydraulics in the core and of the resulting reactivity feedback effects. Initially the core is at the hot zero power state(10^{-6} of full power) of end-of-cycle and the transient occurs by ejecting one control rod in 0.16 sec. There is no reactor scram and after a power excursion the reactor stabilises at a power level determined by the feedback effects. This benchmark is a further development of the benchmark AER-DYN-001 and -002.

The transient core power behaviors obtained for the rod ejection are given in Figure 5-4. One curve in the plot was obtained with 5millisec time step size and the second curve is for more practical case that uses 10 msec for the rapid power change region. The solution accuracy of the two cases are essentially the same and very similar with DYN3D result which is available at the above web site.

The computing time data for each MASTER solution module is given in Table 5-3 for the 10 msec case. The total computation time is about 194 seconds for the 10 sec transient and the spread of the computing time of the three major solution modules is quite reasonable.

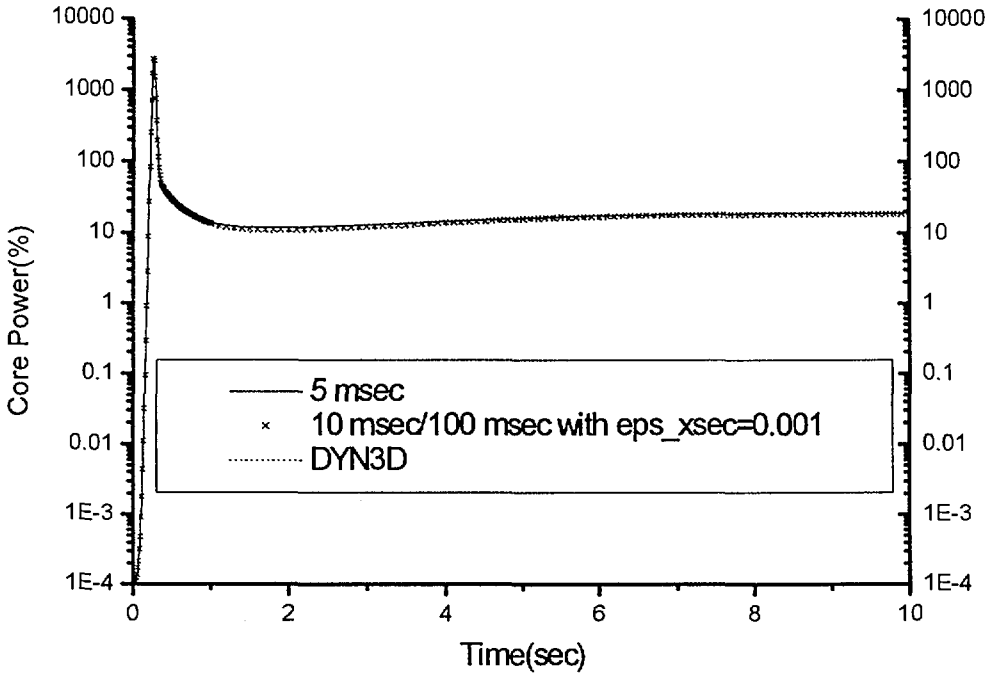

Figure 5-4. Transient Core Powers for the VVER440 Rod Ejection Benchmark

Table 5-3. Computing Time Breakups for the 10 Sec VVER440 Rod Ejection Transient (733 MHz Pentium-III PC, seconds)

CMFD	67.1 (34.7%)
Nodal	39.2 (20.2%)
T/H	78.4 (40.5%)
Miscellaneous	8.9 (4.6%)
Total	193.6 (100.0%)

6. Conclusion

This report is for the implementation of the triangle-based polynomial expansion nodal (TPEN) method to the MASTER code in conjunction with the coarse mesh finite difference(CMFD) framework for hexagonal core design and analysis. In the TPEN method, only two-dimensional triangular domain was considered by expressing axial leakage as a axial source term explicitly. The axial dependence of the intranodal flux was incorporated separately here and it was determined by the nodal expansion method (NEM) for a hexagonal node. To solve the CMFD linear system efficiently, Stabilized Bi-Conjugate Gradient(BiCG) algorithm and Wielandt eigenvalue shift method were adopted. And for the construction of the efficient preconditioner of BiCG algorithm, the incomplete LU(ILU) factorization scheme was used. To apply the ILU factorization scheme to three-dimensional problem, symmetric Gauss-Seidel Factorization scheme was used.

In order to examine the accuracy of the TPEN solution, several eigenvalue benchmark problems and two transient problems, i.e., a realistic VVER1000 and VVER440 rod ejection benchmark problems, were solved and compared with respective references. The results of eigenvalue benchmark problems indicated that non-linear TPEN method was very accurate showing less than 15 pcm of eigenvalue errors and 1% of maximum power errors, and fast enough to solve the three-dimensional VVER-440 problem within 5 seconds on 733 MHz PENTIUM-III. In the case of the transient problems, the non-linear TPEN method also showed quite good results in a few minute of computing time on the same platform machine.

References

[1] Jin-Young Cho, Chang-Hyo Kim, "Higher-Order Polynomial Expansion Nodal Method for Hexagonal Core Neutronics Analysis," Ann. Nucl. Energy, Vol.25, No.13, p1021, 1998.

[2] H. A. Van Der Vorst, "Bl-CGSTAB: A fast and smoothly converging variant of Bl-CG for the solution of nonsymmetric linear systems," SlAM J. Sci. Stat. Comput. 13, pp. 631-644 (1992).

[3] Yousef Saad, Iterative Methods for Sparse Linear Systems, PWS Publishing Co, 1996

[4] Han Gyu Joo, et. al., PARCS: A Multi-Dimensional Two-Group Reactor Kinetics Code Based on the Nonlinear Analytic Nodal Method,PU/NE-98-26 (1998)

[5] Byung-Oh Cho, et.al., "Partial Current Based AFEN Formulation for Hexagonal-Z Neutronics Solver in MASTER," Proc. of International Conference on the Physics of Nuclear Science and Technology, Vol. 2, p980, Long Island, 1998.

[6] Y.A.Chao and Y.A.Shatilla, "Conformal Mapping and Hexagonal Nodal Methods-II: Implementation in the ANC-H Code," Nucl. Sci. Eng. , Vol. **121**, 210-225(1995).

[7] L. Podlazov, et. al., An International Nuclear Safety Center Report, Joint Project #2, Phase 2 Task #7D.

[8] L. Podlazov, et. al., "Coupled Neutronic and Thermal-Hydraulic Code Benchmark Activities at the International Nuclear Safety Center," International Conference on the Physics of Nuclear Science and Technology, p469, Long Island, NY, 1998.

[9] H. S. Khalil, et. Al., "Coupled Reactor Physics and Thermal-Hydraulic Computations with SAS-DIF3DK Code," Proc. Joint Int. Conf. on Mathematical Methods and Supercomputing for Nuclear Application, Vol. 2, p1063, Saratoga Spring, NY, Oct. 5-9, 1997.

[10] O. A. Voronova, et. Al., "Calculations of Multidimensional Test Reactor Neutron Diffusion Problems with KORAT3D Code and Its Combination with Two-Velocity Two-

Temperature Thermal Hydraulic RATEG Code," Proc. Int. Conf. on the Physics of Reactors, PHYSOR 96, Vol. 3, J/119-J/208, Sep. 16-20, 1996.

BIBLIOGRAPHIC INFORMATION SHEET

Performing Org. Report No.	Sponsoring Org. Report No.	Standard Report No.	INIS Subject Code
KAERI/TR-1652/2000			

Title / Subtitle	Non-Linear Triangle-based Polynomial Expansion Nodal Method for Hexagonal Core Analysis
Project Manager and Dept.	Cho, Jin Young (Advanced Reactor Technology Development Team)
Researcher and Dept.	Cho, Byung-Oh (Advanced Reactor Technology Development Team) Joo, Han Gyu (Advanced Reactor Technology Development Team) Zee, Sung-Quun (Advanced Reactor Technology Development Team) Park, Sang Yong (Advanced Reactor Technology Development Team)

Publication Place	**Taejon**	Publisher	**KAERI**	Publication Date	2000.9.
Page	50 p.	Ill. & Tab.	Yes(√), No( )	Size	29.7 cm
Note					

Classified	Open(√), Restricted( ), Class Document	Report Type	Technical Report
Sponsoring Org.		Contract No.	

Abstract (15-20 Lines)

This report is for the implementation of triangle-based polynomial expansion nodal (TPEN) method to MASTER code in conjunction with the coarse mesh finite difference(CMFD) framework for hexagonal core design and analysis. The TPEN method is a variation of the higher order polynomial expansion nodal (HOPEN) method that solves the multi-group neutron diffusion equation in the hexagonal-z geometry. In contrast with the HOPEN method, only two-dimensional intranodal expansion is considered in the TPEN method for a triangular domain. The axial dependence of the intranodal flux is incorporated separately here and it is determined by the nodal expansion method (NEM) for a hexagonal node. For the consistency of node geometry of the MASTER code which is based on hexagon, TPEN solver is coded to solve one hexagonal node which is composed of 6 triangular nodes directly with Gauss elimination scheme.

To solve the CMFD linear system efficiently, stabilized bi-conjugate gradient(BiCG) algorithm and Wielandt eigenvalue shift method are adopted. And for the construction of the efficient preconditioner of BiCG algorithm, the incomplete LU(ILU) factorization scheme which has been widely used in two-dimensional problems is used. To apply the ILU factorization scheme to three-dimensional problem, a symmetric Gauss-Seidel Factorization scheme is used.

In order to examine the accuracy of the TPEN solution, several eigenvalue benchmark problems and two transient problems, i.e., a realistic VVER1000 and VVER440 rod ejection benchmark problems, were solved and compared with respective references. The results of eigenvalue benchmark problems indicate that non-linear TPEN method is very accurate showing less than 15 pcm of eigenvalue errors and 1% of maximum power errors, and fast enough to solve the three-dimensional VVER-440 problem within 5 seconds on 733MHz PENTIUM-III. In the case of the transient problems, the non-linear TPEN method also shows good results within a few minute of computing time on the same platform machine.

Subject Keywords (about 10 words)	Non-Linear Triangle based Polynomial Expansion Nodal Method TPEN , Hexagonal Core, Core Analysis

서 지 정 보 양 식

수행기관보고서번호	위탁기관보고서 번호	표준보고서 번호	INIS 주제코드
KAERI/TR-1652/2000			

제목 / 부제	육방형 노심 해석을 위한 비선형 삼각형 기반 다항식전개법
연구책임자 및 부서명	조 진 영 (동력로기술개발팀)
연 구 자 및 부 서 명	조 병 오 (동력로기술개발팀), 주 한 규 (동력로기술개발팀) 지 성 균 (동력로기술개발팀), 박 상 윤 (동력로기술개발팀)

출 판 지	대전	발행기관	한국원자력연구소	발행년	2000.10.
페 이 지	50 p.	도 표	있음(√),없음( )	크 기	29.7 cm
참고사항	원자력 연구개발 중장기 과제				
비밀여부	공개(√),대외비( ),__급비밀		보고서종류	기술 보고서	
연구위탁기관			계약 번호		

초록 (15-20 줄)

이 연구에서는 육방형 노심 설계/해석을 위한 비선형 다항식전개법을 MASTER 코드에 적용하여 그 성능을 평가하였다. 삼각형노드에 대한 다항식전개 노달법은 3 차원 프리즘노드에 대한 고차다항식전개법과 유사한 방법으로 축방향으로의 중성자누설항을 중성자 확산방정식에서 중성자원으로 두어 고차다항식전개법에서의 축방향 노드간의 연계를 차단한 방법이다. 축방향으로의 중성자원은 노달전개법(NEM)을 도입하여 구하였다. 그리고 MASTER 코드의 노드구조와 일치시키기 위해 6 개의 삼각형으로 구성된 하나의 육각형 노드에 대한 다항식 전개법의 해를 가우스소거법에 의해 직접 푸는 방식을 채택하였다.

거시격자 유한차분법의 해를 효율적으로 구하기 위한 방법으로는 Stabilized Bi-Conjugate Gradient(BiCG) 알고리듬과 Wielandt eigenvalue shift 방법이 채택되었다. 그리고 BiCG 알고리듬의 선행자(preconditioner)를 구하기 위해서 불완전 LU 인자법(incomplete LU factorization)이 사용되었으며 이를 3 차원 공간에 적용하기 위해 symmetric Gauss-Seidel Factorization 방법이 사용되었다.

비선형 다항식 전개법의 정확도 및 계산속도 검증은 다양한 고유치 계산문제와 2 개의 과도해석문제를 통해 수행되었다. 고유치문제에 대한 적용결과 비선형 다항식전개법은 모든 문제에서 15pcm 이내의 고유치 오차를 그리고 최대 1% 이내의 집합체 출력오차를 보여 매우 정확한 방법임을 보였으며, VVER-440 3 차원 문제를 5 초이내에 계산하여 매우 빠른 방법임을 보였다. 과도해석문제에 대해서는 다른 코드 결과와 매우 유사한 결과를 보였으며 수분이내에 계산을 완료하여 매우 빠름을 확인하였다.

주제명키워드 (10 단어내외)	비선형 삼각형 기반 다항식전개법, 육방형 노심, 노심해석